

## PAPER

View Article Online  
View Journal | View IssueCite this: *J. Mater. Chem. B*, 2015, 3,  
1813Silica-coated Au@ZnO Janus particles and their  
stability in epithelial cells†Moritz Susewind,<sup>a</sup> Anna-Maria Schilmann,<sup>a</sup> Julia Heim,<sup>b</sup> Andreas Henkel,<sup>c</sup>  
Thorben Link,<sup>d</sup> Karl Fischer,<sup>c</sup> Dennis Strand,<sup>b</sup> Ute Kolb,<sup>c</sup> Muhammad Nawaz Tahir,<sup>a</sup>  
Jürgen Brieger<sup>b</sup> and Wolfgang Tremel<sup>\*a</sup>

Multicomponent particles have emerged in recent years as new compartmentalized colloids with two sides of different chemistry or polarity that have opened up a wide field of unique applications in medicine, biochemistry, optics, physics and chemistry. A drawback of particles containing a ZnO hemisphere is their low stability in biological environment due to the amphoteric properties of Zn<sup>2+</sup>. Therefore we have synthesized monodisperse Au@ZnO Janus particles by seed-mediated nucleation and growth whose ZnO domain was coated selectively with a thin SiO<sub>2</sub> layer as a protection from the surrounding environment that imparts stability in aqueous media while the Au domain remained untouched. The thickness of the SiO<sub>2</sub> layer could be precisely controlled. The SiO<sub>2</sub> coating of the oxide domain allows biomolecule conjugation (e.g. antibodies, proteins) in a single step for converting the photoluminescent and photocatalytic active Janus nanoparticles into multifunctional efficient vehicles for cell targeting. The SiO<sub>2</sub>-coated functionalized nanoparticles were stable in buffer solutions and other aqueous systems. Biocompatibility and potential biomedical applications of the Au@ZnO@SiO<sub>2</sub> Janus particles were assayed by a cell viability analysis by co-incubating the Au@ZnO@SiO<sub>2</sub> Janus particles with epithelia cells and compared to those of uncoated ZnO.

Received 8th December 2014  
Accepted 5th January 2015

DOI: 10.1039/c4tb02017k

www.rsc.org/MaterialsB

## Introduction

There is a plethora of procedures available for crafting the sizes, shapes, or surface chemistries of nanocrystals. Spheres, polyhedra, rods, plates, tetrapods, or dumbbells can be made with high fidelity.<sup>1</sup> These nanocrystals can be functionalized using organic ligands with functionalities imparting specific surface properties: solubility, specificity towards small molecules or larger biomolecules,<sup>2</sup> resilience to nonspecific adsorption,<sup>3</sup> electric charge,<sup>4</sup> or electrochemical activity.<sup>5</sup> A particularly interesting group of nanomaterials are asymmetric (Janus-type) heteroparticles, compartmentalized colloids that possess two ends of different polarity and/or chemistry.

Janus particles have attracted attentions in a wide range of applications<sup>6</sup> and they are fascinating objects in the study of self-assembly,<sup>7,8</sup> in the stabilization of emulsions,<sup>9,10</sup> as dual-functionalized optical, electronic, and sensor devices.<sup>11,12</sup> Janus particles have been obtained first from dendrimers<sup>13,14</sup> and block copolymer micelles,<sup>15,16</sup> but later also from inorganic nanoparticles containing gold,<sup>17–21</sup> silver,<sup>17,18,22,23</sup> platinum,<sup>24–26</sup> alloys,<sup>27–31</sup> or 3d metals,<sup>32–35</sup> and oxide, metal and metal sulfide<sup>36–44</sup> components, or semiconductor NPs.<sup>45</sup>

The interesting features of Janus particles are attributed to their tunable asymmetric structure, which allows controlling their physicochemical properties down to the nanoscale. Catalytically or electrochemically active metal components (e.g. Au, Pt, or Ni)<sup>46,47</sup> and magnetic materials have received attention, because the noble metals can be recovered magnetically after use. In addition, wavelength-tunable photocatalytic materials with efficient charge separation capabilities have been made with heterostructures based nanocrystals with size-tunable properties.<sup>48,49</sup>

When loaded with distinct drugs or dyes, the particles have potential biomedical applications.<sup>50</sup> In addition their potential for multiplexing, multilevel targeting, and combination therapies makes them active targets of research.<sup>50,51</sup> Janus particles with adjustable composition and form may have multiple functionalities that are useful for synchronous biolabeling, separation, detection, and multimodal imaging in biomedicine.<sup>50–53</sup> A

<sup>a</sup>Institut für Anorganische Chemie und Analytische Chemie, Johannes Gutenberg-Universität, Duesbergweg 10-14, D-55099 Mainz, Germany. E-mail: tremel@uni-mainz.de; tahir@uni-mainz.de; Fax: +49 6131 39-25605; Tel: +49 6131 39-25135

<sup>b</sup>Hals-, Nasen-Ohrenklinik, Universitätsmedizin der Johannes Gutenberg Universität Mainz, Langenbeckstr. 1, D-55131 Mainz, Germany

<sup>c</sup>Institut für Physikalische Chemie, Johannes Gutenberg-Universität, Welderweg 11, 55099 Mainz, Germany

<sup>d</sup>Institut für Physiologische Chemie, Abteilung Angewandte Molekularbiologie, Johannes Gutenberg-Universität, Duesbergweg 6, D-55099 Mainz, Germany

† Electronic supplementary information (ESI) available. See DOI: 10.1039/c4tb02017k

stringent requirement is a highly controlled synthesis to obtain Janus particles with well defined structural, physical, chemical and toxicological properties.

Au nanoparticles, the prototypical metal component of Janus particles, show a large polarizability in the optical range *via* excitation of localized surface plasmon resonances,<sup>54,55</sup> and they generate a strong optical signal. The fluorescence from the Au nanoparticles may originate from radiative recombination of sp-band electrons and d band holes, which could be enhanced by 4–6 orders of magnitude due to the surface plasmons of nanocrystals or rough metal surfaces. Previously, Au nanorods have shown strong two-photon fluorescence for cellular imaging.<sup>56–64</sup>

Furthermore, they are very stable and can bind molecules of interest in a controlled fashion without photobleaching, a typical drawback of common fluorescent dyes.<sup>65</sup> In addition, gold nanoparticles have promising therapeutic properties as hyperthermal agents because the local temperature around gold nanoparticles can be increased by laser illumination through the tunable surface plasmon bands in the near infrared region (NIR).<sup>66–68</sup>

Among the metal oxides, ZnO is an important transparent semiconductor which has been explored for applications such as solar cells,<sup>69–71</sup> optoelectronic devices,<sup>72</sup> or for cell labeling in biological applications<sup>73</sup> or for the promotion of reactive oxygen species generation.<sup>56,74</sup> Moreover, they have shown some promise as cholesterol biosensors, dietary modulators for hydrolase activity relevant to controlling diabetes and hyperlipaemia, as well as cell imaging.

One major drawback of semiconductor particles such as ZnO is their instability in non-neutral media. As a result, ZnO nanoparticles are mildly toxic in organisms<sup>57–60</sup> which is related to dissolution of  $\text{Zn}^{2+}$  ions. In contrast, ligand coated nanoparticles, however, have shown lower toxic effects depending on the constitution of the protection shell.<sup>21,61</sup> Therefore, the formation of a silica coating around the ZnO component may offer advantages such as chemical and physical protection from the surrounding environment, stability in aqueous media, and a platform for further modification,<sup>62,63</sup> but a continuous silica shell around the Janus particles would forfeit the surface addressability of a heteroparticle.<sup>64</sup>

Here, we present a method for the synthesis of multifunctional Au@ZnO Janus particles, where only the ZnO component was covered with a thin silica shell due to the wetting of the hydrophilic ZnO compared to the hydrophobic Au component. The established surface chemistry for silica still allowed adapting the particle properties through specific functionalization by conjugation of chromophores or biomolecules. Different from uncoated Au@ZnO or pure ZnO nanocrystals Au@ZnO@SiO<sub>2</sub> Janus particles were stable in human blood serum and epithelial cells. Their solubility in physiological medium, good biocompatibility and fluorescence in combination with optical activity imparted by the Au component makes them alternatives to current nanoparticle-platforms for biomedical/bioimaging applications. Intrinsically fluorescent silica coated Au@ZnO nanocrystals were water-soluble (Fig. S1, ESI†) and could be adopted for molecularly targeted imaging of cancer cells *in vitro*.

## Experimental

Zinc acetate dihydrate (99.999% trace metals basis Sigma Aldrich), gold(III) chloride hydrate (99.999% trace metals basis Sigma Aldrich), benzyl alcohol, (99%, Acros) oleylamine (90%, Acros), i-octadecene (90%, Acros), Igepal CO-520 (Sigma Aldrich), tetraethoxysilane (TEOS) (>99%, Sigma Aldrich), fluorescein 5(6)-isothiocyanate (FITC) (Sigma Aldrich), rhodamine B isothiocyanate (RITC) (Sigma Aldrich), ammonium hydroxide (25%, aqueous solution, Sigma Aldrich), 2-methoxy-(polyethyleneoxy)-propyltrimethoxysilane (PEG-silane,  $n = 6-9$ ) (90%, ABCR), cyclohexane (Sigma Aldrich), ethanol (99.8%, Roth), chloroform (>99%, Sigma Aldrich), hexane (p.A. Fisher), imidazole (99%, (titration), crystalline, Sigma Aldrich), were used as received without further purification.

### Synthesis of Au@ZnO hybrid nanocrystals

Au@ZnO hybrid nanocrystals were synthesized by mixing 0.05 mmol of gold(III) chloride hydrate (20 mg), 6 mL of benzyl alcohol, 3 mL of 1-octadecene, 3 mL oleylamine, and 0.5 mmol of zinc acetate dihydrate (109 mg, pre-annealed at 110 °C for 10 min), and the mixture was heated to 120 °C. The reaction contents were kept at 120 °C for 20 min. The solution was further heated to 180 °C and kept at this temperature for 30 min and cooled slowly to room temperature. The product was precipitated from solution by centrifugation (9000 rpm, 10 min, RT). Finally, the product was dissolved in chloroform or hexane and stored at room temperature.

### Synthesis of ZnO nanocrystals

ZnO nanocrystals were synthesized by dissolving 0.5 mmol of zinc acetate dihydrate (109 mg and preheated at 110 °C for 10 min) in 7 mL of benzyl alcohol and 3 mL of oleylamine. The mixture was heated slowly to 180 °C and kept at this temperature for 30 min. The nanoparticles were precipitated with excess ethanol and separated by centrifugation. Finally, the product was dissolved in chloroform or hexane and stored at room temperature.

### Surface functionalization of ZnO nanoparticles and Au@ZnO hybrid nanocrystals

ZnO or Au@ZnO hybrid nanocrystals (1.6 mg) were dissolved in 1 mL of  $\text{CHCl}_3$  and mixed with 3 mL of imidazole solution (1 mg mL<sup>-1</sup>). The solution was stirred for 5 min at room temperature under inert gas conditions. The functionalized Au@ZnO heterostructures were precipitated by centrifugation and subsequently washed twice with ethanol and finally resuspended in distilled water.

### Silica coating of Au@ZnO hybrid nanocrystals

The SiO<sub>2</sub> functionalization was performed using the reverse microemulsion technique. Briefly, 200 mg of Igepal-CO-520 were dissolved in 3.5 mL cyclohexane and stirred for 10 min under Ar-atmosphere. Then roughly 1.6 mg of the Au@ZnO nanoparticles in 70  $\mu\text{L}$  of *n*-hexane were added to the solution

and stirred for further 30 min. Aqueous  $\text{NH}_4\text{OH}$  (18  $\mu\text{L}$ ) were added to induce micelle formation. TEOS (14  $\mu\text{L}$ ) (and FITC) were added after 4 min and the reaction mixture proceeded under Ar-atmosphere over night.

### Functionalization of $\text{Au@ZnO@SiO}_2$ nanocrystals

Further functionalization of the silica shell was achieved by addition of PEG-silane (15  $\mu\text{L}$ ), which led to complete precipitation of the  $\text{Au@ZnO@SiO}_2$  nanoparticles within 2 h. The nanoparticles were collected by centrifugation and washed several times by dissolution in ethanol and centrifugation (13 000 rpm, 10 min, RT). The obtained particles were easily soluble in acetone, ethanol, DMF/DMSO, and various aqueous media.

### Analytical characterization

The particles were characterized by transmission electron microscopy (TEM), attenuated total reflection Fourier transformed infrared spectroscopy (ATR-FT-IR), UV-Vis, photoluminescence and fluorescence spectroscopy, dark field microscopy (DFM) and dynamic light scattering (DLS). TEM images were recorded using a Philips EM420 microscope with an acceleration voltage of 120 kV. Further a FEI Tecnai F-30 TEM with an acceleration voltage of 300 kV with field emission and EDX and EELS detectors was used for the HR-TEM images. Samples for TEM were prepared by dropping a dilute solution of nanoparticles in the appropriate solvent (hexane, ethanol, water) onto a carbon coated copper grid (Plano, Wetzlar; Germany). ATR-FT-IR-spectra were measured on a Thermo Scientific Nicolet iS10 FT ATR-IR spectrometer. UV-Vis-spectra were collected by a Varian Cary 5000 UV-Vis/NIR-spectrometer, the photoluminescence spectra were recorded on a Horiba Jobin Yvon-SPEX (Fluoro Max-2) fluorescence spectrometer and the fluorescence analysis was performed with an Olympus AHB3 light microscope, together with an AH3-RFC-reflected light fluorescence attachment at the emission wavelength of 540 nm. DFM measurements were performed on a Zeiss Axio Observer Z1 inverted microscope with a PI542 XY-piezo stage. Furthermore, an Inspector V10E transmissive imaging spectrograph with an Andor Luca R EM-CCD was added. The true colour images were taken with a Canon EOS 5D Mark II (IR-filter removed). The automated data acquisition for the 33 single scattering spectra was performed with a MATLAB based control software. For the two-photon analysis a Zeiss LSM 710 NLO microscope equipped with Non Descanned Detectors (NDDs) and a Coherent Chameleon Ultra II Ti:Sapphire Laser was used. The image acquisition was performed with a LD C-Apochromat 40x/1.1 W Korr M27 objective, and the samples were excited at 832 nm. Seventy percent laser power 30 mW was used. The emitted fluorescence was passed through 455–500, 500–550, and 610–656 nm band-pass filters to NDDs. All data were acquired and processed using ZEN 2009 software (Carl Zeiss, Germany).

### Dynamic light scattering (DLS)

DLS measurements were performed using a Uniphase He/Ne Laser ( $\lambda = 632.8$  nm, 22 mW), a ALV-SP125 Goniometer, a ALV/

High QE APD-Avalanche photo-diode with fiber optical detection, a ALV 5000/E/PCi-correlator and a Lauda RC-6 thermostat unit. Angular dependent measurements were carried out in the range  $30^\circ \leq \theta \leq 150^\circ$ . For data evaluation experimental intensity correlation functions were transformed into amplitude correlation functions applying the Siegert-relation extended to include negative values after baseline subtraction from  $g_1(t) = \text{SIGN}(G_2(t)) \cdot \text{SQRT}(\text{ABS}((G_2(t) - A)/A))$ .

$g_1(t)$  was obtained by fitting a biexponential function  $g_1(t) = a \exp(-t/b) + c \exp(-t/d)$  which accounts for the sample polydispersity. Average apparent diffusion coefficients  $D_{\text{app}}$  were determined from the equation  $q^2 \cdot D_{\text{app}} = (a \cdot b^{-1} + c \cdot d^{-1})/(a + c)$ .  $D_{\text{app}}(q = 0)$  was determined by plotting  $D_{\text{app}}(q)$  vs.  $q^2$  and extrapolation to  $q \rightarrow 0$ . Hydrodynamic radii were extracted from the Stokes–Einstein equation. Sample concentrations for the DLS measurements were in the range  $0.2 \text{ g L}^{-1}$ . All samples were filtered into dust free cylindrical scattering cells (Hellma, Suprasil, 2 cm diameter) using syringe filters (Millipore LCR 450 nm for aqueous solutions).

### Cell culture and cytotoxicity-assay

An adenocarcinoma cell line A549 (ATCC, Manassas, VA, USA) was used as a model of respiratory epithelia. Cells were cultured in DMEM/Ham's F12 (Sigma Aldrich), supplemented with 5% FCS (Sigma Aldrich) and antibiotic solution (100  $\text{U mL}^{-1}$  penicillin and 100  $\mu\text{g mL}^{-1}$  streptomycin; Sigma Aldrich) at  $37^\circ\text{C}$  in 5%  $\text{CO}_2$ . For analysis of the cell viability after treatment with the  $\text{Au@ZnO@SiO}_2$  nanoparticles, 15.000 cells per well were seeded in a 96 well plate and cultivated overnight for adherence. Next day, the cells were treated with the Janus particles in three different concentrations (25, 50 and 100  $\mu\text{g mL}^{-1}$ ) for 24 h. After incubation, 100  $\mu\text{L}$  70% ice cold EtOH was added to the cells of the death control for 10 min. The media of all wells were replaced by 200  $\mu\text{L}$  FCS-medium with 10% Alamar Blue (Biozol Diagnostica, Eching, Germany). Subsequently the samples were incubated for 3 h at  $37^\circ\text{C}$ . The results were obtained using a (Fluoroskan Ascent Microplate reader, Thermo Fisher Scientific GmbH, Rockford, USA) plate reader (ex: 540 nm, em: 600 nm) and normalized to untreated control. After measuring the viability of the cells, the results had to be compared to the real cell number per well. For this, the cells were washed 3 times with PBS and a 0.2% crystal purple solution (50  $\mu\text{L}$  per well) was added and incubated for 10 min at  $37^\circ\text{C}$ . After incubation the cells were washed again and were treated with 40  $\mu\text{L}$  of 10% acetic acid for lysis. The real cell amount was measured on plate reader (Mikrotiterplattenphotometer Multiskan Ascent®, Thermo Fisher Scientific GmbH, Rockford, USA) at 540 nm.

### Immunofluorescence staining

The cells were fixed (4% paraformaldehyde, methanol free) and washed 3 times with PBS and nonspecific interactions were blocked for 20 min in 1% BSA/PBS. Afterwards, cells were exposed to phalloidin (5  $\mu\text{L}/200 \mu\text{L}$  v/v, Cell Signaling, Danvers, USA) for 20 min. The coverslips were mounted on slides using DAKO fluorescent mounting medium (Dako, Inc., Carpinteria,



CA, USA). All slides were examined using an inverted microscope (Nikon ECLIPSE TE2000-U).

## Results and discussion

Au@ZnO Janus particles were prepared following a recently reported method.<sup>75</sup> The synthetic route for the preparation of the nanoparticles and its encapsulation with the silica shell is illustrated in Fig. 1. In the first step Au nanoparticle intermediates were prepared *in situ* by reduction of  $[\text{AuCl}_4]^-$  in the presence of oleylamine at 120 °C. ZnO was nucleated heterogeneously on the gold seeds and grown by thermal decomposition of zinc acetate at ~180 °C. Match-stick-type Au@ZnO hybrid nanocrystals were prepared in the nonpolar solvent 1-octadecane.

The silica encapsulation of Janus particles *via* reverse microemulsion technique has been employed previously.<sup>21,63</sup> The particular challenge for Au@ZnO is the instability of the ZnO component in acidic or basic media due to the amphoteric character of Zn. It exerts a strong influence on the Au/ZnO interface as well, *i.e.* in the silica-encapsulating step a well-defined and visible silica shell must be formed without changing the Janus particle morphology.

The thickness of the silica shell could be controlled by adjusting the pH value. The hydrolysis of TEOS is increased by catalytic amounts of acid or base. We deposited silica by basic hydrolysis of TEOS in dilute  $\text{NH}_3$  solution. By varying the pH of the aqueous phase the thickness of the silica shell could be precisely controlled in the nanometer range: for pH = 10.3 the shell thickness was 1–2 nm, at pH = 10.9 it increased to 3–4 nm (Fig. 2a–d) as determined by TEM.

The Au domains were not wetted due to their hydrophobicity, and the silica shell forms exclusively on the metal oxide domains as confirmed by TEM (Fig. S3, ESI<sup>†</sup>) and TEM-EDX (Fig. S4, ESI<sup>†</sup>), thereby leaving the Au domains available for further functionalization, *e.g.* with thiols. The TEM data for individual particles are corroborated for bulk samples by quantitative evaluation of the X-ray diffraction data of Au@ZnO hybrid nanocrystals (Rietveld refinements) (Fig. S2, ESI<sup>†</sup>). Only single nanoparticles were encapsulated in a silica shell, multiple encapsulations were not observed. Fig. 2 shows Au@ZnO@SiO<sub>2</sub> nanoparticles after the functionalization was complete. The nanoparticles appear uniform and well separated, even though, they are functionalized orthogonally.

The formation of the silica shell was monitored by FT-IR spectroscopy. Fig. 3 displays FT-IR-spectra of Au@ZnO nanoparticles before and after silica encapsulation. The spectrum of

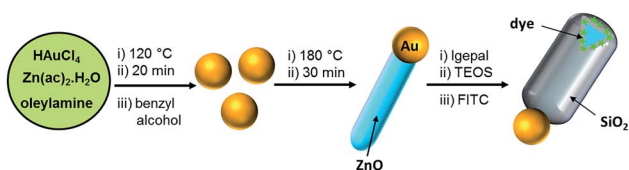


Fig. 1 Seed-mediated growth of Au@ZnO Janus particles and subsequent silica encapsulation of the ZnO domain.

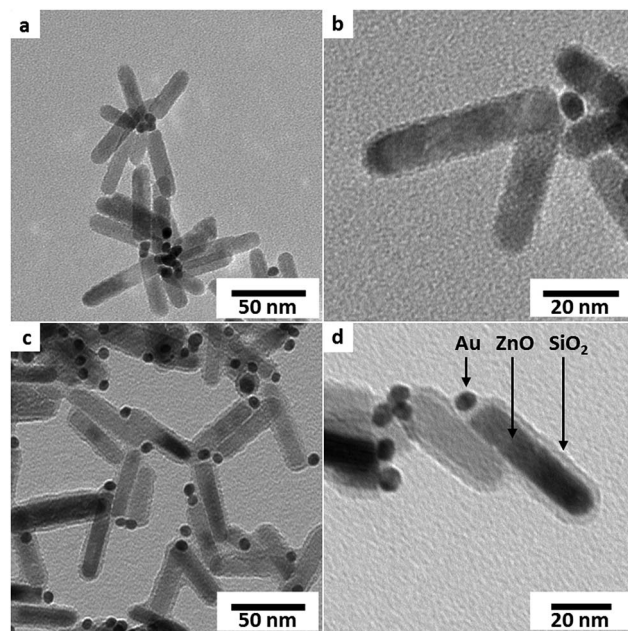


Fig. 2 (a) Overview TEM bright field image of Au@ZnO@SiO<sub>2</sub> nanoparticles showing aggregation *via* the hydrophobic Au tips, (b) corresponding TEM micrograph of single encapsulated heterodimers with 2 nm silica shell thickness and (c and d) particle aggregation and morphology of Au@ZnO@SiO<sub>2</sub> with 4 nm shell thickness.

oleylamine-capped Au@ZnO nanoparticles (black line) displays characteristic vibrational bands at 2926 and 2854  $\text{cm}^{-1}$ , which are assigned the symmetric and asymmetric stretching modes of the  $\text{CH}_2$ - and  $\text{CH}_3$ -groups.<sup>76</sup> In the IR spectrum of the Au@ZnO@SiO<sub>2</sub> particles, a broad and strong band system in the region between 1200 and 1000  $\text{cm}^{-1}$  appeared, which can be assigned to the O–Si–O stretching modes. The stretching vibrations due to  $\text{CH}_2$ - and  $\text{CH}_3$ -groups remained, although less

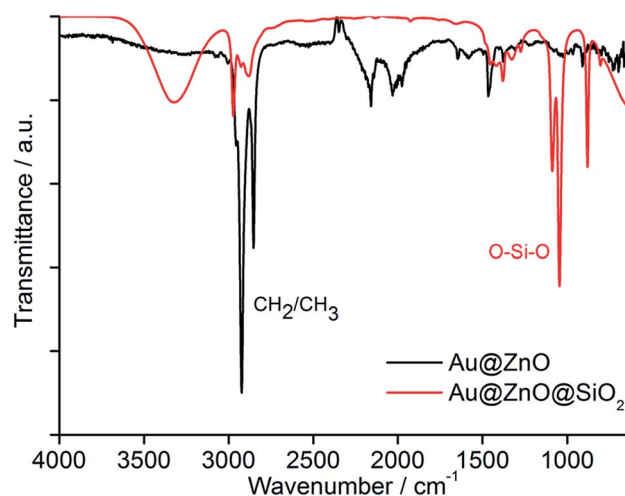


Fig. 3 Fourier transform infrared (FT-IR) spectra of Au@ZnO (black line) and Au@ZnO@SiO<sub>2</sub> (red line) nanoparticles. Strong O–Si–O stretching modes emerge with silica encapsulation of the nanoparticles.

pronounced, due to the conjugation of PEG-chains to the surface of the silica shell as well as the ligands of the Au domains.<sup>63</sup>

The UV/Vis absorption spectra of Au@ZnO@SiO<sub>2</sub> Janus particles in Fig. 4a show two absorption maxima: the ZnO semiconductor is excited at 355 nm,<sup>77</sup> while the Au plasmon band appears at 494 nm. Au nanoparticles in the 5–12 nm size range show a characteristic plasmon resonance at  $\approx$ 512–520 nm, where the exact maximum depends on the particle shape and surface coating.<sup>21,54</sup> There is an increase of the ZnO absorbance intensity of Au@ZnO@SiO<sub>2</sub> compared to the spectrum of uncoated Au@ZnO (Fig. 4a), additionally photoluminescence spectroscopy was performed on that sample. Excitation of the ZnO domain at 325 nm wavelength showed a much stronger intensity of the Au@ZnO@SiO<sub>2</sub> than of the Au@ZnO nanoparticles (Fig. 4b). This is in line with an earlier report on ZnO nanoparticles incorporated in a silica matrix.<sup>78</sup>

The exciton band of pure ZnO nanoparticles appears at 360 nm, and is slightly red shifted for 5 nm. The quasi-epitaxial growth of the ZnO domains on the gold seeds changes the local dielectric function of their surrounding medium, and therefore, the position of the maximum of the plasmon absorption band.

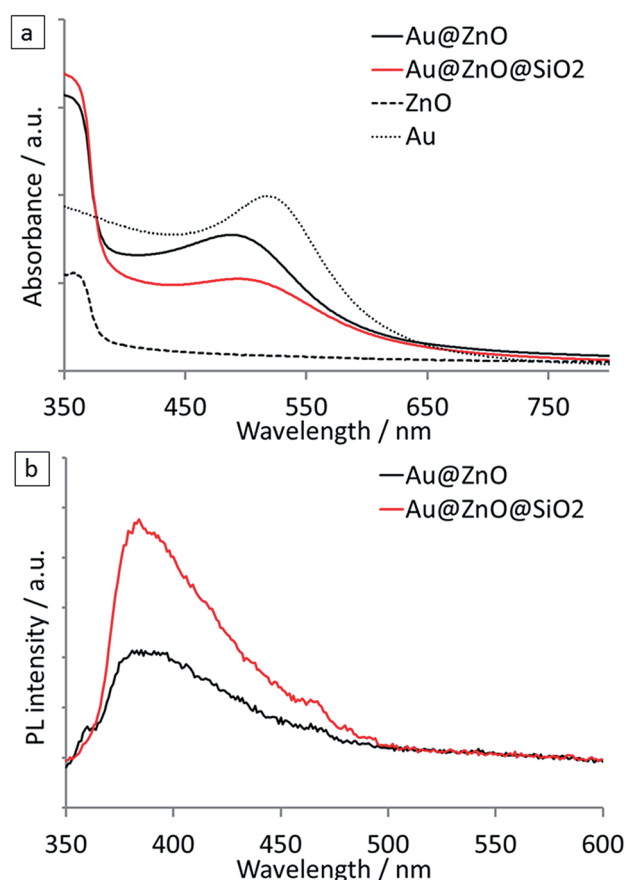


Fig. 4 (a) UV-Vis spectra of Au@ZnO (solid, black), Au (dotted, grey) and ZnO (dotted, black) and Au@ZnO@SiO<sub>2</sub> (solid, red) nanoparticles. The silica layer thickness of the encapsulated nanoparticles is 1–2 nm. (b) Photoluminescence spectra of Au@ZnO (solid, black) and silica encapsulated Au@ZnO@SiO<sub>2</sub> (solid, red) nanoparticles after excitation with light of 325 nm wavelength.

Fig. 4a shows a blue shift of the absorption maximum of the gold components by about 25 nm compared to the plasmon band of pure Au nanoparticles ( $\approx$ 512–520 nm depending on parameters like particle morphology, size, solvent according to Mie's theory).<sup>79,80</sup> The shift may be estimated quantitatively using the optical constants for Au nanoparticles and is related by the conjugation to semiconducting ZnO, the dependence of the wavelength on the density of electrons, effective electron mass, as well as shape and size of charge distribution.<sup>81</sup>

The Au@ZnO@SiO<sub>2</sub> nanoparticles showed a bright fluorescence under UV light suggesting an application as fluorescent probe. The green emission of ZnO is believed to originate from defects, such as oxygen vacancies in a form of a singly ionized  $V_O^+$  centers or a doubly ionized  $V_O^{++}$  centers, zinc vacancies or interstices, are possible causes of the green emissions in ZnO. The silica shell inhibits the diffusion of reactive species from the surface to the ZnO core, although the protection may be incomplete due to the presence of micropores in the shell. The PL spectrum of the Au@ZnO@SiO<sub>2</sub> nanoparticles in Fig. 4b shows a broad signal with an emission peak at 385 nm when excited with light of 325 nm, which can be attributed to the ZnO domain according to the literature.<sup>82</sup> Besides the diverse addressability of the two domains with biomolecules on the Au part and dyes in the silica shell respectively, the particles therefore serve as optical detection agents in two different wavelength regions. To further probe the two-photon activity of the Janus particles without any dye incorporated in the shell the particles were excited using a wavelength of 832 nm. Fig. 5 shows the fluorescence images with emissions on the blue, green and red channel. The strong emission on the blue channel compared to the green and red one fits well with the enhancement of photoluminescence by the ZnO domain in this wavelength regime. The usage of ZnO as one part of the Janus particles thereby serves as support for a silica shell which can be addressed with different dyes on the one hand and second enhances emissions in the blue wavelength region. The two-photon activity with excitation at 832 nm provides cell targeting with low cell damage at simultaneously strong emissions in the blue wavelength regime.

Further spectroscopic investigation of the Au@ZnO@SiO<sub>2</sub> particles by dark field microscopy (DFM) revealed an aggregation in polar solvents. More than thirty single scattering spectra of these aggregates were recorded according to the literature;<sup>83</sup> all of them showed a bimodal form with very similar resonance positions, as displayed for four representative spectra in Fig. 6a. All spectra were recorded by DFM from the sample in Fig. 6b. The TEM micrograph also indicated similar aggregation of the nanoparticles which stick together *via* their Au tips in order to avoid hydrophilic/hydrophobic interactions (Fig. 6c). The amplitude of the scattering spectra consists of two optical modes, which have been reported for smaller aggregates of noble metal nanoparticles,<sup>84</sup> generating two plasmon resonances. The individual spectra were taken from aggregates attached to a glass surface from original solution without drying, so they reflect the state in solution. According to the spectra for silver nanoparticle trimers<sup>84</sup> and TEM micrograph

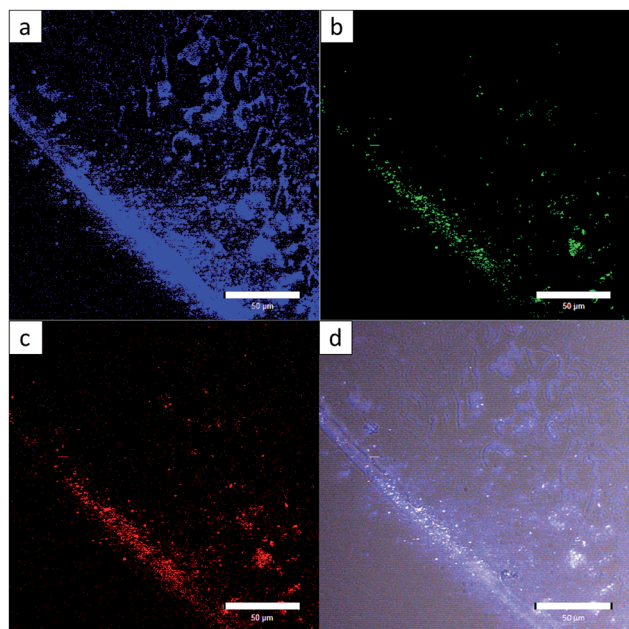


Fig. 5 Two-photon fluorescence of Au@ZnO@SiO<sub>2</sub>: (a)–(c) fluorescence images on the blue, green and red channel, (d) overlay image of all channels including light microscopy image. Excitation laser wavelength: 832 nm, Scale: 50 μm.

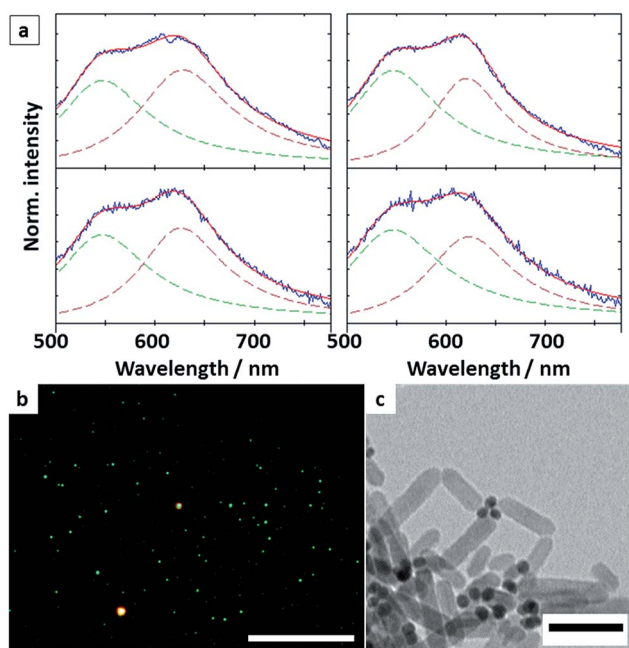


Fig. 6 (a) Darkfield microscopy scattering spectra (scattering spectrum (blue, solid), Lorentzian fit-functions of single modes (dashed), superposition of Lorentzian fits (red, solid)), taken from the image (b, scale: 20 μm) indicate aggregation of the Janus particles via their gold tips as shown in (c). Scale: 50 nm.

analysis (Fig. 6c), the particles might aggregate in the form of fully symmetric trimers.

A better insight into the aggregation behaviour of the particles in solution was obtained from dynamic light scattering

(DLS) measurements of aqueous nanoparticle solutions ( $c = 0.2 \text{ g L}^{-1}$ ) at five different scattering angles in the range of  $30^\circ \leq \theta \leq 150^\circ$  (Fig. 7). Fig. 7a displays nearly monomodal decay functions, indicating a relative low polydispersity. In a regime, where for monodisperse particles the product of the scattering vector  $q$  and the rod length  $L$  is  $\leq 5$ , one should expect a mono-exponential decay of the amplitude correlation function  $g_1(t)$ . The average rod length of 60 nm was determined by TEM; it results in a  $qL$  regime of  $qL \leq 1.5$ . The expected diffusion coefficient  $D$  can be calculated by an expression given by Tirado and Garcia de la Torre,<sup>85</sup> whereby

$$D = \frac{kT}{3\pi\eta L} (\ln p + v) \quad (1)$$

with

$$v = 0.312 + \frac{0.565}{p} - \frac{0.1}{p^2} \quad (2)$$

Here,  $p$  is the aspect ratio ( $L/d$ ) of the nanorods with the rod length  $L$  (60 nm) and the diameter  $d$  (10 nm). The calculation of

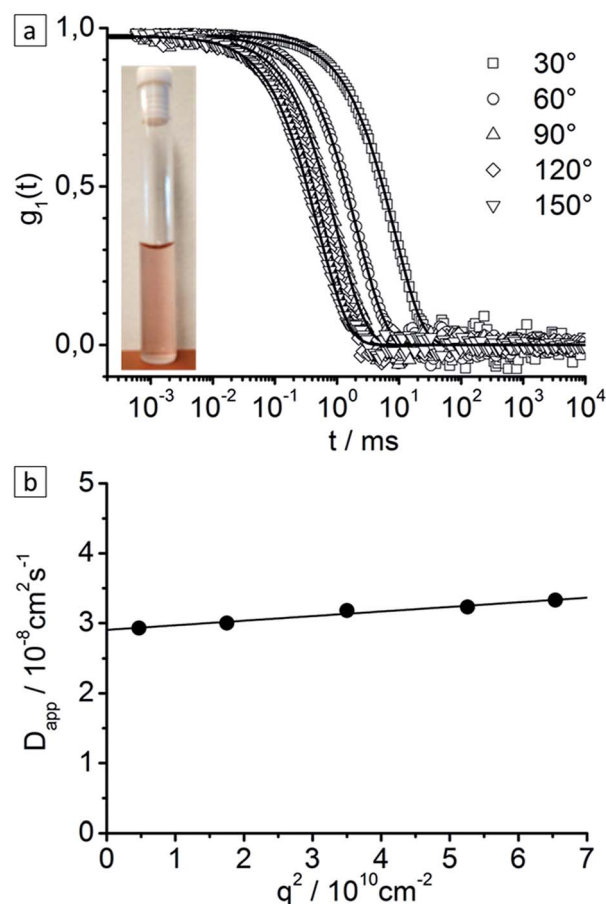


Fig. 7 (a) Biexponential fits (solid line) of the amplitude correlation functions at five different scattering angles showing nearly mono-modal decay (Au@ZnO@SiO<sub>2</sub> in Millipore water,  $0.2 \text{ g L}^{-1}$ ,  $T = 293 \text{ K}$ , viscosity  $\eta$ : 1.005 cP) (b) apparent diffusion coefficient as a function of the squared scattering vector  $q^2$  in the range of  $30^\circ \leq \theta \leq 150^\circ$ .



the hydrodynamic radius  $R_H$  from the diffusion coefficient  $D_s$  is given by the Stokes–Einstein equation

$$D_s = \frac{kT}{6\pi\eta R_H} \quad (3)$$

which yields a calculated hydrodynamic radius

$$R_H = \frac{L}{2(\ln p + \nu)} \quad (4)$$

for anisotropic nanoparticles. For the aspect ratio  $p = 6$  and the parameter  $\nu = 0.4$ , the expected hydrodynamic radius is  $R_H = 14$  nm. From the z-average diffusion coefficient  $\langle D_s \rangle_z$  for  $q = 0$  (Fig. 7b), the hydrodynamic radius was calculated by the Stokes–Einstein equation, yielding  $R_H = 74$  nm. The disparity between the theoretical and experimental value suggests also some aggregation behaviour in solution. Micellar arrangement seems to be very homogenous according to the nearly mono-exponential decay functions in Fig. 7. The really low polydispersity of the samples is further confirmed by an only slight angular dependency of the apparent diffusion coefficient, which is only  $\sim 5\%$  over the whole angular range (Fig. 7b). This low polydispersity gives evidence for the existence of well defined aggregates, which may be considered to be “micellar like”. Since hydrodynamic radii were nearly the same for measurements with and without low salt concentrations (50 mM TBS; 5 mM NaCl), the aggregation seems to be independent of Coulomb interactions.

These results follow the explanation of hydrophobic Au-tip/Au-tip arrangements to avoid hydrophobic/hydrophilic interactions. In order to further prove the free addressability of the Au-tip, an orthogonal functionalization was performed on the Au domain *via* the Au specific isothiocyanate group of the dye Rhodamine B isothiocyanate (RITC). The silica shell was tagged with FITC dye during silica formation; RITC was bound on the Au tip afterwards. Fig. 8 displays the UV-Vis spectrum of the orthogonal dye tagged nanoparticles. The absorbance maxima of FITC (492 nm) and RITC (550 nm) clearly emerge in the absorbance spectrum of the functionalized nanoparticles.

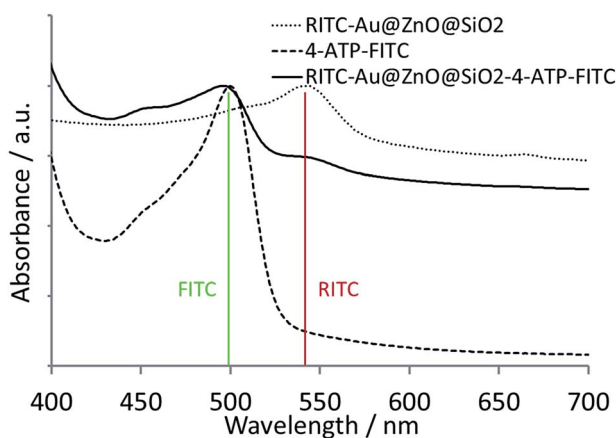


Fig. 8 UV-Vis spectra of orthogonal functionalized Janus nanoparticles with the dyes FITC (incorporated into the silica shell) and RITC (bound to the Au domain) (solid) and spectra of the single components (dashed).

The functionalized particles with incorporated FITC dye were analyzed by fluorescence microscopy to visualize the silica coated ZnO domains (Fig. 9). The images show aggregates of nanoparticles upon excitation with blue light ( $\lambda = 490$  nm). Reference samples without dye showed no fluorescence.

### Biocompatibility of the particles

A potential biomedical use of silica coated Au@ZnO Janus particles is the targeted drug delivery using immunostimulatory oligonucleotides.<sup>50,63,86–88</sup> Therefore, the cytotoxic behavior of the Au@ZnO@SiO<sub>2</sub> Janus particles was studied for human adenocarcinoma cells (A549).

Biocompatibility and potential biomedical applications of the Au@ZnO@SiO<sub>2</sub> Janus particles were assayed by a cell viability analysis by co-incubating the Au@ZnO@SiO<sub>2</sub> Janus particles with the adenocarcinoma A549 cell line. A cell viability assay (for 24 h, 37 °C) revealed the Au@ZnO@SiO<sub>2</sub> Janus particles to be non-cytotoxic, *i.e.* that in concentrations of 25, 50, and 100  $\mu\text{g mL}^{-1}$  the percentage of cell survival was in all cases  $\geq 90\%$  (Fig. 10). Contrary, ZnO nanoparticles without a silica protection shell revealed a much lower cell viability of  $\sim 20\%$  (100  $\mu\text{g mL}^{-1}$ ). The drastically reduced cell toxicity of the encapsulated Janus nanoparticles *in vitro* is

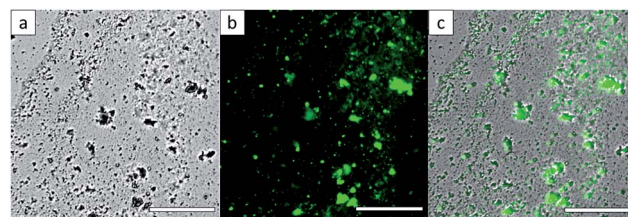


Fig. 9 (a) Light microscope image of Au@ZnO@SiO<sub>2</sub> nanoparticle aggregates, (b) corresponding confocal laser fluorescence scanning microscopy image with embedded FITC dye excited with 490 nm, (c) overlay image of (a) and (b). Scale: 50  $\mu\text{m}$ .

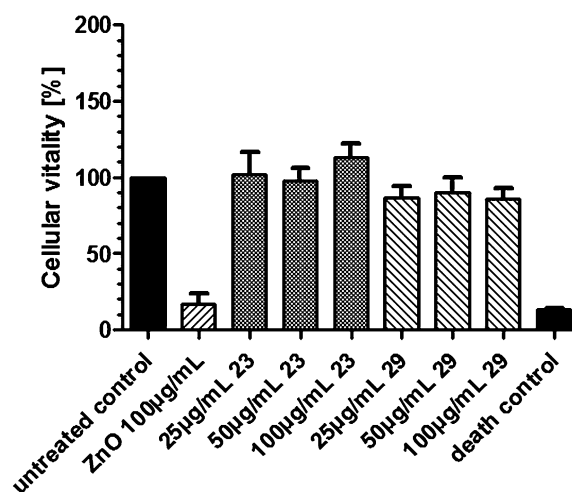


Fig. 10 Vitality assay of A549 cells incubated with non-toxic Au@ZnO@SiO<sub>2</sub> nanoparticles. Contrary, pure ZnO nanoparticles (100  $\mu\text{g mL}^{-1}$ ) behave mildly cell toxic and show little cell viability ( $\sim 20\%$ ).

supposed to originate from the prevented dissolution of Zn ions which potentially enables the heterodimers to act as stable, non-toxic molecules in cell targeting. To demonstrate the cell uptake, immunofluorescence staining was successfully performed with FITC-labeled Au@ZnO@SiO<sub>2</sub> in Alexa Fluor 555 Phalloidin-labeled adenocarcinoma cells (Fig. S5, ESI†).

### Immunofluorescence staining

Cell imaging was carried out by confocal laser fluorescence scanning microscopy. For immunofluorescence staining, the cells were cultivated and incubated overnight in order to achieve full coverage on the coverslips. The next day the cells were co-incubated for 24 h with FITC-labeled Au@ZnO@SiO<sub>2</sub> with a final concentration of 100 µg mL<sup>-1</sup>. The confocal laser fluorescence scanning microscopy image displays the uptake of the green fluorescent Janus nanoparticles in the Alexa-labeled adenocarcinoma cells (red) (Fig. S5, ESI†).

## Conclusions

In summary, we demonstrated the synthesis of well-defined anisotropic Janus nanoparticles consisting of a Au noble metal and a ZnO domain acting as potential non-cytotoxic cell targeting molecules in the UV and visible wavelength regime. The ZnO part could selectively be encapsulated with a thin silica shell in order to stabilize the nanoparticles in aqueous systems and to prevent the particles from ion leaching. Contrary to pure ZnO nanoparticles, which are mildly cell toxic and show only little cell survival percentages of ~20% in cell viability assays, the cytotoxicity of the Au@ZnO@SiO<sub>2</sub> Janus nanoparticles is drastically reduced with cell viability percentages of ≥90% (100 µg mL<sup>-1</sup> in each case). The thickness of the shell could be adjusted *via* the pH-value of the micelle inducing aqueous ammonia solution during the silica forming step. TEM analysis and various spectroscopic methods revealed self-aggregation *via* the Au tips due to hydrophobic/hydrophobic interactions, thereby indicating the orthogonal silica encapsulation leaving the Au domains untouched for subsequent functionalization *e.g.* with thiol bearing biopolymers. The synthesized Janus particles exhibited good colloidal stability in aqueous systems, such as Millipore water, TBS buffer and physiological media, thus enabling the nanoparticles to serve as biocompatible and multifunctional heterodimers with a drastically reduced cytotoxicity *in vitro* in contrast to ZnO nanoparticles. Besides their biocompatibility the Au@ZnO@SiO<sub>2</sub> Janus particles also have great potential as fluorophores in the field of cell targeting through the Au plasmon band, the enhanced photoluminescence intensity of the ZnO domain and the possibility to incorporate fluorescence dyes into the silica shell. Confocal laser fluorescence scanning microscopy images of the uptake of FITC-labeled nanoparticles in adenocarcinoma cells demonstrated their potential to use them as suitable cell targeting molecules.

## Acknowledgements

This research was supported by the Deutsche Forschungsgesellschaft through the SFB 1066. We are grateful to Professor Manfred Schmidt for technical support regarding DLS measurements. The facilities of the Electron Microscopy Center in Mainz (EZMZ) were supported by the State Excellence Cluster COMATT and SFB 625. Microscopy work of the LSM-Core Facility at the University Clinic in Mainz was supported by the Research Center for Immunology (FZI).

## Notes and references

- 1 L. Carbone and P. D. Cozzoli, *Nano Today*, 2010, **5**, 449–493.
- 2 E. Katz and I. Willner, *Angew. Chem., Int. Ed.*, 2004, **43**, 6042–6108.
- 3 M. Zheng, F. Davidson and X. Huang, *J. Am. Chem. Soc.*, 2003, **125**, 7790–7791.
- 4 A. M. Kalsin, M. Fialkowski, M. Paszewski, S. K. Smoukov, K. J. M. Bishop and B. A. Grzybowski, *Science*, 2006, **312**, 420–424.
- 5 T. G. Drummond, M. G. Hill and J. K. Barton, *Nat. Biotechnol.*, 2003, **21**, 1192–1199.
- 6 D. Wang and Y. Li, *Adv. Mater.*, 2011, **23**, 1044–1060.
- 7 S. Mann, *Nat. Mater.*, 2009, **8**, 781–792.
- 8 A. Walther and A. H. E. Müller, *Chem. Rev.*, 2013, **113**, 5194–5261.
- 9 P. Dommersnes, Z. Rozynek, A. Mikkelsen, R. Castberg, K. Kjerstad, K. I. Hersvik and J. O. Fossum, *Nat. Commun.*, 2013, **4**, 2066.
- 10 D. Hirsemann, S. Shylesh, R. A. De Souza, B. Diar-Bakerly, B. Biersack, D. N. Mueller, M. Martin, R. Schobert and J. Breu, *Angew. Chem.*, 2012, **124**, 1376–1380; *Angew. Chem., Int. Ed.*, 2012, **51**, 1348–1352.
- 11 A. Perro, S. Reculosa, S. Ravaine, E. Bourgeat-Lami and E. Duguet, *J. Mater. Chem.*, 2005, **15**, 3745–3760.
- 12 A. G. Vanakaras, *Langmuir*, 2006, **22**, 88–93.
- 13 J. Ropponen, S. Nummelin and K. Rissanen, *Org. Lett.*, 2004, **6**, 2495–2497.
- 14 V. Percec, M. R. Imam, T. K. Bera, V. S. K. Balagurusamy, M. Peterca and P. A. Heiney, *Angew. Chem.*, 2005, **117**, 4817–4823; *Angew. Chem., Int. Ed.*, 2005, **44**, 4739–4745.
- 15 J. Wang, G. Liu and G. Rivas, *Anal. Chem.*, 2003, **75**, 4667–4671.
- 16 R. Erhardt, M. F. Zhang, A. Böker, H. Zettl, C. Abetz, P. Frederik, G. Krausch, V. Abetz and A. H. E. Müller, *J. Am. Chem. Soc.*, 2003, **125**, 3260–3267.
- 17 H. Yu, M. Chen, P. M. Rice, S. X. Wang, R. White and S. Sun, *Nano Lett.*, 2005, **5**, 379–382.
- 18 C. Xu, J. Xie, D. Ho, C. Wang, N. Kohler, E. Walsh, J. Morgan, Y. Chin and S. Sun, *Angew. Chem.*, 2008, **120**, 179–182; *Angew. Chem., Int. Ed.*, 2008, **47**, 173–176.
- 19 C. Xu, B. Wang and S. Sun, *J. Am. Chem. Soc.*, 2009, **131**, 4216–4217.
- 20 T. D. Schladt, M. I. Shukoor, M. N. Tahir, F. Natalio, K. Schneider, I. Ament, J. Becker, F. Jochum, S. Weber, P. Theato, L. M. Schreiber, C. Sönnichsen, H.-C. Schröder,



- W. E. G. Müller and W. Tremel, *Angew. Chem.*, 2010, **122**, 4068–4072; *Angew. Chem., Int. Ed.*, 2010, **49**, 3976–3980.
- 21 I. Schick, S. Lorenz, D. Gehrig, A.-M. Schilman, H. Bauer, M. Panthöfer, K. Fischer, M. Schmidt, D. Strand, F. Laquai and W. Tremel, *J. Am. Chem. Soc.*, 2014, **136**, 2473–2483.
- 22 C. Pacholski, A. Kornowski and H. Weller, *Angew. Chem.*, 2004, **116**, 4878–4881; *Angew. Chem., Int. Ed.*, 2004, **43**, 4774–4777.
- 23 F. R. Fan, Y. Ding, D.-Y. Liu, Z. Q. Tian and Z. L. Wang, *J. Am. Chem. Soc.*, 2009, **131**, 12036–12037.
- 24 H. Gu, Z. Yang, J. Gao, C. Chang and B. Xu, *J. Am. Chem. Soc.*, 2005, **127**, 34–35.
- 25 S. H. Choi, H. B. Na, Y. I. Park, A. Kwangjin, S. G. Kwon, Y. Jang, M.-H. Park, J. Moon, J. S. Son, C. I. Song, M. W. Moon and T. Hyeon, *J. Am. Chem. Soc.*, 2008, **130**, 15573–15580.
- 26 H. Hong, L. Hu, M. Li, J. Zheng, X. Sun, X. Lu, X. Cao, J. Lu and H. Gu, *Chem.-Eur. J.*, 2011, **17**, 8726–8730.
- 27 A. Figuerola, A. Fiore, R. Di Corato, A. Falqui, C. Gianni, E. Micotti, A. Lascialfari, M. Corti, R. Cingolani, T. Pellegrino, P. D. Cozzoli and L. Manna, *J. Am. Chem. Soc.*, 2008, **130**, 1477–1487.
- 28 T. D. Schladt, T. Graf, O. Köhler, H. Bauer, K. Schneider, C. Herold, J. Mertins and W. Tremel, *Chem. Mater.*, 2012, **24**, 525–535.
- 29 M. Casavola, V. Grillo, E. Carlino, F. Gozzo, E. F. Pinel, M. A. Garcia, L. Manna, R. Cingolani and P. D. Cozzoli, *Nano Lett.*, 2007, **7**, 1386–1395.
- 30 M. R. Buck, J. F. Bondi and R. E. Schaak, *Nat. Chem.*, 2012, **4**, 37–44.
- 31 M. J. Bradley, A. J. Biacchi and R. E. Schaak, *Chem. Mater.*, 2013, **25**, 1886–1892.
- 32 B. Nakhjavan, M. N. Tahir, H. Gao, T. D. Schladt, K. Schneider, F. Natalio, I. Ament, R. Branscheid, S. Weber, H.-C. Schröder, W. E. G. Müller, U. Kolb, C. Sönnichsen, L. M. Schreiber and W. Tremel, *J. Mater. Chem.*, 2011, **21**, 8605–8611.
- 33 B. Nakhjavan, M. N. Tahir, M. Panthöfer, H. Gao, T. Gasi, V. Ksenofontov, R. Branscheid, S. Weber, U. Kolb, L. M. Schreiber and W. Tremel, *Chem. Commun.*, 2011, **47**, 8898–8900.
- 34 B. Nakhjavan, M. N. Tahir, F. Natalio, M. Panthöfer, H. Gao, M. Dietzsch, R. Andre, T. Gasi, V. Ksenofontov, R. Branscheid, U. Kolb and W. Tremel, *Nanoscale*, 2012, **4**, 4571–4577.
- 35 T. Mokari, E. Rothenberg, I. Popov, R. Costi and U. Banin, *Science*, 2004, **304**, 1787–1790.
- 36 T. Mokari, C. G. Sztrum, A. Salant, E. Rabani and U. Banin, *Nat. Mater.*, 2005, **4**, 855–863.
- 37 A. E. Saunders, I. Popov and U. Banin, *J. Phys. Chem. B*, 2006, **110**, 25421–25429.
- 38 G. Menagen, D. Mocatta, A. Salant, I. Popov, D. Dorfs and U. Banin, *Chem. Mater.*, 2008, **20**, 6900–6902.
- 39 W. Shi, H. Zeng, Y. Sahoo, T. Y. Ohulchanskyy, Y. Ding, Z. L. Wang, M. Swihart and P. N. Prasad, *Nano Lett.*, 2006, **6**, 875–881.
- 40 J. Yang, E. I. Elim, Q. Zhang, J. Y. Lee and W. Ji, *J. Am. Chem. Soc.*, 2006, **128**, 11921–11926.
- 41 J. Yang, L. Levina, E. H. Sargent and S. O. Kelley, *J. Mater. Chem.*, 2006, **16**, 4025–4028.
- 42 D. V. Talapin, H. Yu, E. V. Shevchenko, A. Lobo and C. B. Murray, *J. Phys. Chem. C*, 2007, **111**, 14049–14054.
- 43 J.-S. Lee, E. V. Shevchenko and D. V. Talapin, *J. Am. Chem. Soc.*, 2008, **130**, 9673–9675.
- 44 J. Yang and J. Y. Ying, *Chem. Commun.*, 2009, 3187–3189.
- 45 C. G. Read, A. J. Biacchi and R. E. Schaak, *Chem. Mater.*, 2013, **25**, 4304–4311.
- 46 W. Teunissen, A. Bol and J. W. Geus, *Catal. Today*, 1999, **48**, 329–336.
- 47 S. Shylesh, V. Schünemann and W. R. Thiel, *Angew. Chem.*, 2010, **122**, 2913–2917; *Angew. Chem., Int. Ed.*, 2010, **49**, 3428–3459.
- 48 P. V. Kamat, *J. Phys. Chem. C*, 2007, **111**, 2834–2860.
- 49 R. Costi, A. E. Saunders and U. Banin, *Angew. Chem.*, 2010, **122**, 4996–5016; *Angew. Chem., Int. Ed.*, 2010, **49**, 4878–4897.
- 50 T. D. Schladt, K. Schneider, H. Schild and W. Tremel, *Dalton Trans.*, 2011, **40**, 6315–6343.
- 51 L. Carbone and P. D. Cozzoli, *Nano Today*, 2010, **5**, 449–493.
- 52 D. Yoon, J. H. Lee, T.-H. Shin and J. Cheon, *Acc. Chem. Res.*, 2011, **44**, 863–874.
- 53 N. Kamaly, Z. Xiao, P. M. Valencia, A. F. Radovic-Moreno and O. C. Farokhzad, *Chem. Soc. Rev.*, 2012, **41**, 2971–3010.
- 54 J. Perez-Juste, I. Pastoriza-Santos, L. M. Liz-Marzan and P. Mulvaney, *Coord. Chem. Rev.*, 2005, **249**, 1870–1901.
- 55 M. Hu, J. Chen, Z. Y. Li, L. Au, G. V. Hartland, X. Li, M. Marquez and Y. Xia, *Chem. Soc. Rev.*, 2006, **35**, 1084–1094.
- 56 H. Yin and P. S. Casey, *Langmuir*, 2010, **26**, 15399–15408.
- 57 M. Mortimer, K. Kasemets and A. Kahrua, *Toxicology*, 2010, **269**, 182–189.
- 58 M. Heinlaan, A. Ivask, I. Blinova, H. C. Dubourguier and A. Kahru, *Chemosphere*, 2008, **71**, 1308–1316.
- 59 H. H. Wang, R. L. Wick and B. S. Xing, *Environ. Pollut.*, 2009, **157**, 1171–1177.
- 60 V. Aruoja, H. C. Dubourguier, K. Kasemetsa and A. Kahru, *Sci. Total Environ.*, 2009, **407**, 1461–1468.
- 61 H. J. Zhang, H. M. Xiong, Q.-G. Ren, Y.-Y. Xia and J.-L. Kong, *J. Mater. Chem.*, 2012, **22**, 13159–13165.
- 62 Y. K. Peng, C.-W. Lai, C.-L. Liu, H.-C. Chen, Y.-H. Hsiao, W.-L. Liu, K.-C. Tang, Y. Chi, J.-K. Hsiao, K. E. Lim, H.-E. Liao, J.-J. Shyue and P.-T. Chou, *ACS Nano*, 2011, **5**, 4177–4187.
- 63 T. D. Schladt, K. Koll, S. Prüfer, H. Bauer, F. Natalio, O. Dumele, R. Raidoo, S. Weber, U. Wolfrum, L.-M. Schreiber, M. P. Radsak, H. Schild and W. Tremel, *J. Mater. Chem.*, 2011, **22**, 9253–9262.
- 64 G. A. Sotiropoulos, A. M. Hirt, P.-Y. Lozach, A. Teleki, F. Krumeich and S. E. Pratsinis, *Chem. Mater.*, 2011, **23**, 1985–1992.
- 65 D. Boyer, P. Tamarat, A. Maali, B. Lounis and M. Orrit, *Science*, 2002, **297**, 1160–1163.
- 66 X. Huang, I. H. El-Sayed, W. Qian and M. A. El-Sayed, *J. Am. Chem. Soc.*, 2006, **128**, 2115–2120.
- 67 R. S. Norman, J. W. Stone, A. Gole, C. J. Murphy and T. L. Sabo-Attwood, *Nano Lett.*, 2008, **8**, 302–306.

- 68 E. B. Dickerson, E. C. Dreaden, X. Huang, I.-H. El-Sayed, H. Chu, S. Pushpanketh, J. F. McDonald and M. A. El-Sayed, *Cancer Lett.*, 2008, **269**, 57–66.
- 69 Q. Zhang, T. P. Chou, B. Russo, S. A. Jenekhe and G. Cao, *Angew. Chem.*, 2008, **120**, 2939–2949; *Angew. Chem., Int. Ed.*, 2008, **47**, 2402–2406.
- 70 N. Memarian, I. Concina, A. Braga, S. M. Rozati, A. Vomiero and G. Sberveglieri, *Angew. Chem.*, 2011, **123**, 12529–12533; *Angew. Chem., Int. Ed.*, 2011, **50**, 12321–12325.
- 71 A. Kim, Y. Won, K. Woo, C.-H. Kim and J. Moon, *ACS Nano*, 2013, **7**, 1081–1091.
- 72 G. G. Huang, C. T. Wang, H. T. Tang, Y. S. Huang and J. Yang, *Anal. Chem.*, 2006, **78**, 2397–2404.
- 73 X. Tang, E. S. G. Tang, L. Li, J. Ding and J. Xue, *Chem. Mater.*, 2010, **22**, 3383–3388.
- 74 G. Applerot, A. Lipovsky, R. Dror, N. Perkash, Y. Nitzan, R. Lubart and A. Gedanken, *Adv. Funct. Mater.*, 2009, **19**, 842–852.
- 75 M. N. Tahir, F. Natalio, M. A. Cambaz, M. Panthöfer, R. Branscheid, U. Kolb and W. Tremel, *Nanoscale*, 2013, **5**, 9944–9949.
- 76 T. D. Schladt, T. Graf and W. Tremel, *Chem. Mater.*, 2009, **21**, 3183–3190.
- 77 P. Li, Z. Wei, T. Wu, Q. Peng and Y. Li, *J. Am. Chem. Soc.*, 2011, **133**, 5660–5663.
- 78 Z. Fu, B. Yang, L. Li, W. Dong, C. Jia and W. Wu, *J. Phys.: Condens. Matter*, 2003, **15**, 2867–2873.
- 79 G. Mie, *Ann. Phys.*, 1908, **330**, 377–445.
- 80 M.-C. Daniel and D. Astruc, *Chem. Rev.*, 2004, **104**, 293–346.
- 81 K. L. Kelly, E. Coronado, L. L. Zhao and G. C. Schatz, *J. Phys. Chem. B*, 2003, **107**, 668–677.
- 82 E. V. Chelnokov, N. Bityurin, I. Ozerov and W. Marine, *Appl. Phys. Lett.*, 2006, **89**, 171119.
- 83 C. Rosman, J. Prasad, A. Neiser, A. Henkel, J. Edgar and C. Sönnichsen, *Nano Lett.*, 2013, **13**, 3243–3247.
- 84 D. W. Brandl, N. A. Mirin and P. Nordlander, *J. Phys. Chem. B*, 2006, **110**, 12302–12310.
- 85 M. M. Tirado and J. Garcia de la Torre, *J. Chem. Phys.*, 2003, **119**, 9914–9920.
- 86 M. I. Shukoor, F. Natalio, P. Gupta, M. Wiens, M. Tarantola, M. Barz, S. Weber, M. Terekhov, H.-C. Schröder, W. E. G. Müller, A. Janshoff, P. Theato, R. Zentel, L.-M. Schreiber and W. Tremel, *Adv. Funct. Mater.*, 2009, **9**, 3717–3725.
- 87 M. I. Shukoor, F. Natalio, N. Glube, M. N. Tahir, H. A. Therese, V. Ksenofontov, N. Metz, P. Theato, P. Langguth, J.-P. Boissel, H.-C. Schröder, W. E. G. Müller and W. Tremel, *Angew. Chem.*, 2008, **120**, 4826–4830; *Angew. Chem., Int. Ed.*, 2008, **47**, 4748–4752.
- 88 M. I. Shukoor, F. Natalio, T. D. Schladt, K. Koll, M. N. Tahir, M. Barz, S. Weber, C. Brochhausen, R. Zentel, M. Wiens, L.-M. Schreiber, J. Brieger, W. E. G. Müller and W. Tremel, *J. Mater. Chem.*, 2011, **22**, 8826–8834.